buildings

MDPI

Article

A Fast-Calibrated Computational Fluid Dynamic Model for Timber–Concrete Composite Ventilated Façades

Sofia Pastori [1], Mohammed-Sadegh Salehi [2,3], Stefan Radl [3,*] and Enrico Sergio Mazzucchelli [1]

[1] Politecnico di Milano, Department of Architecture, Built Environment and Construction Engineering, Via Ponzio 31, 20133 Milano, Italy; sofia.pastori@polimi.it (S.P.); enrico.mazzucchelli@polimi.it (E.S.M.)
[2] VIRTUAL VEHICLE Research Center, Inffeldgasse 21a, 8010 Graz, Austria; m.salehi@tugraz.at
[3] Institute of Process and Particle Engineering, Graz University of Technology, Inffeldgasse 13/III, 8010 Graz, Austria
* Correspondence: radl@tugraz.at

Abstract: Timber–concrete composite (TCC) systems join the positive aspects of engineered wood products (good seismftaic behaviour, low thermal conductivity, environmental sustainability, good behaviour under fire if appropriately designed) with those of concrete (high thermal inertia, durability, excellent fire resistance). TCC facades are typically composed of an internal insulated timber-frame wall and an external concrete slab, separated by a ventilated air cavity. However, there is very limited knowledge concerning the performance of TCC facades, especially concerning their thermal behaviour. The present paper deals with the development and optimization of a 2D Computational Fluid Dynamic (CFD) model for the analysis of TCC ventilated façades' thermal behaviour. The model is calibrated and validated against experimental data collected during the annual monitoring of a real TCC ventilated envelope in the north of Italy. Also, a new solver algorithm is developed to significantly speed up the simulation (i.e., 45 times faster simulation at an error below 3.5 °C compared to a typical CFD solver). The final model can be used for the time-efficient analysis (simulation time of approximately 23 min for a full day in real-time) and the optimization of the thermal performance of TCC ventilated facades, as well as other ventilated facades with external massive cladding. Our simulation strategy partially avoids the expensive and time-consuming construction of mock-ups, or the use of comparably slow (conventional) CFD solvers that are less suitable for optimization studies.

Keywords: ventilated façade; CFD; timber–concrete composite façade; timber-based construction; thermal performance

Citation: Pastori, S.; Salehi, M.-S.; Radl, S.; Mazzucchelli, E.S. A Fast-Calibrated Computational Fluid Dynamic Model for Timber–Concrete Composite Ventilated Façades. *Buildings* **2024**, *14*, 3567. https://doi.org/10.3390/buildings14113567

Academic Editors: Jiying Liu and Jie Deng

Received: 2 August 2024
Revised: 31 October 2024
Accepted: 4 November 2024
Published: 9 November 2024

1. Introduction

In recent years, the building sector has been characterized by rapid growth in the use of engineered wood products (EWPs) thanks to their great properties related to seismic behaviour, thermal insulation, environmental sustainability, their behaviour under fire (if designed in appropriate way), the positive attitude towards prefabrication and systems integration, and the possibility of disassembly at the end of life [1]. However, EWPs are also characterized by a fragile stress–strain behaviour, high hygroscopicity, and low durability if not properly protected [2]. In the context of building envelopes, lightweight timber facades have a low thermal inertia and poor acoustic performance when compared to alternatives with a higher mass. In contrast, massive timber solutions involve a significant consumption of virgin material and have high costs. To overcome some of the material limits and achieve an improved behaviour in terms of mechanical properties, acoustic performance, fire resistance, and durability, timber structures are sometimes integrated with concrete, resulting in timber–concrete composite (TCC) systems [3].

TCC facades are usually composed by an internal highly insulated timber wall coupled with an external concrete slab acting as a shield against the weather [4], particularly in

the case of extreme weather events like windstorms and hailstorms. Such composite facades join the positive aspects of EWPs (i.e., reduced weight, good thermal insulation, sustainability, ease of prefabrication and systems integration, nice esthetics, etc.) with those of concrete (i.e., good mechanical resistance, high thermal inertia, good acoustic insulation, excellent durability, fire resistance, etc.) [5]. Also, they can lead to innovative esthetic solutions for off-site timber-based construction since the presence of a concrete slab allows for the application of heavy materials (e.g., tiles, stones), or the reproduction of 2D/3D patterns and textures as external finishings.

Besides off-site timber-based construction, nowadays another widely discussed topic concerns the use of ventilated façades and their advantages in terms of their thermal, acoustic, and water-tightness properties [6]. TCC facades can be ventilated facades. In this case, the presence of an air cavity between the timber wall and the concrete slab is needed to separate between the external (potentially humid) concrete slab and the internal insulated timber wall. The latter must always be dry to prevent material degradation. Moreover, several research studies in the literature highlight the good thermal behaviour of ventilated facades during summer, thanks to the presence of an air flow into the cavity (i.e., the chimney effect). This flow can remove some of the energy input to the façade due to solar irradiation [6–8].

A detailed assessment of the thermal performance of ventilated façades is a current issue within research since their interaction with the external environment is complex and requires experimental tests and a Computational Fluid Dynamics (CFD) analysis of the air flow inside the cavity [9]. Many papers in the literature deal with the assessment of ventilated facades thermal behaviour trough experimental and numerical analysis [7,8]: considering the studies published in the last 20 years, most of the research contributions in the literature involve experimental monitoring, followed by analytical analysis and CFD modelling. However, the latter only involves validation against experimental results in a few cases. Unless unexpected errors occur in the sensors measurements, experimental monitoring produces results consistent with reality, but at the same time strictly related to the specific case study [9]. On the one hand, analytical methods have been used for a long time, and their reliability has been shown by a great number of studies. They are simplified procedures based on physical correlations whose reliability has been verified over time [10]. On the other hand, CFD simulations allow us to reach a higher level of detail (i.e., spatially resolved results), but since they have been introduced more recently, there is a limited body of previous studies. This leads to a major uncertainty and to the need for validation against experimental results [4]. The combined use of experimental analysis and CFD modelling is seen as the most complete and precise procedure to assess the thermal behaviour of ventilated facades [9]. It is exactly the use of this combination that motivates our present study on ventilated facades with external massive cladding. Specifically, we study a TCC envelope, for which very little research is present in the literature [4,11], and no rigorous CFD modelling studies were found. Thus, further research is needed to fully understand the thermal behaviour of TCC ventilated façades with external massive cladding, which is the focus of our present study.

1.1. Ventilated Facades CFD Modelling

The CFD technique has been widely used for air flow simulation in the cavity of ventilated facades. Such a simulation models the air flow with a system of governing equations representing continuity, momentum, turbulence, enthalpy, and concentration [12]. The system of equations is solved for all nodes of a 2D or 3D grid to provide detailed information about the nature of the flow field. This numerical approach uses the Finite Difference Method (FDM) or the Finite Volume Method (FVM) to solve the equations.

One of the main problems related to the application of the CFD approach to the building physics domain is the computing power [13]. This limitation led to CFD studies being restricted to steady-state or very short dynamic periods [14–16].

Pasut and De Clari [17] discussed relevant and negligible factors in CFD simulations of naturally ventilated facades, in order to reduce the computational cost. The authors also highlighted that for natural ventilated facades the velocity field is almost bidirectional, hence 3D models are not needed.

Since CFD can provide precise information about the nature of the flow field, it is useful for understanding the effect of details in the design of a ventilated facade. For example, the flow around venetian blinds [18], openings [19], and different shading systems [20] has been studied. Specifically, the latter study by Baldinelli [20] validated a 2D CFD model against experimental results, proving that the use of a 2D instead of a 3D approach gave a negligible additional error.

CFD is useful because it can be integrated (i.e., "coupled") with building energy simulations (BESs) to provide complementary information on the building's performance. However, there are some challenges when integrating BES and CFD analysis [21]: the timescale, the modelling, and the speed discontinuity. The first is produced because the typical characteristic timescale of BES is within the order of few hours, while for CFD it is a few seconds. The modelling discontinuity appears since the air temperature is spatially averaged in BES models but represented as a spatially resolved field in CFD. Finally, the speed discontinuity produces a huge difference in the computing time needed for each model. In summary, coupled BES-CFD simulations take much longer computing time than BESs alone. The corresponding numerical results are more accurate, especially when calculating convective heat transfer coefficients [22].

To speed up ventilated facades CFD analysis, some authors performed single-region simulations, where the solid layers of the façade were simplified by using a 1D approach, e.g., in the work of Pastori et al. [4]. More recent work [23] performed multi-region simulations, i.e., so-called "conjugate heat transfer" (CHT) simulations, where the temperature distribution in all solids is also computed co-currently with the flow problem cases. Such simulations are also available for indoor flow problems [24]. In some cases, calibration is required to overcome the problem of unknown parameters and boundary conditions, e.g., in the field of BESs [25]. Previously, the calibration of a CFD model was performed by Hajdukiewicz [26]. However, she only considered the flow domain (i.e., air), and assumed adiabatic wall boundary conditions and a steady-state flow. Unfortunately, when modelling TCC ventilated facades, the strategy by Hajdukiewicz [26] is not useful, since the solid regions act as the main storage for thermal energy, and a steady state does not exist.

Considering ventilated facades with massive cladding, e.g., TCC ventilated facades, a multi-region approach and transient analysis are required for a complete understanding of the thermal behaviour. A calibration study of a transient multi-region CFD simulation model is not available in the available literature. Such transient multi-region simulations are considerably more computationally expensive, since the region with the largest thermal relaxation time (i.e., that with the slowest thermal response) dictates the number of time steps to be performed.

1.2. Objectives

The central goal of the research was the development of a multi-region transient CFD model to describe the thermal performance of TCC ventilated façades and its calibration and validation against experimental results. Specifically, the first sub-goal was to implement the model and a novel algorithm for time stepping by using the CFD solver OpenFOAM (OpenFOAM® v2206 was used, see Appendix A for details). Similarly to Laitinen et al. [27] and Chourdakis et al. [28], the solver "chtMultiRegionFoam" was used as the basis for the work. The key novelty of the time-stepping algorithm developed is a significant simulation speed up compared to a conventional time stepping solver. The second sub-goal was to perform a sensitivity analysis of the model's prediction accuracy compared to the real façade's behaviour, with respect to key input parameters (i.e., the physical properties and boundary conditions applied). The final goal was model calibration by considering a key

input parameter (i.e., the heat capacity of one solid region), and its validation against the experimental results collected by monitoring the real behaviour of the façade [29].

The innovative aspect of our research is the combination of a fast multi-region CFD model with a calibration procedure. This combination allows for the implementation of relatively fast calibration workflows that enhance the predictive capabilities of, e.g., digital twins in the future.

2. Materials and Methods

The research focuses on the study of the thermal behaviour of the prefabricated TCC ventilated façade system in Figure 1. The system is composed of an internal timber frame structure coupled with an external 50 mm thick reinforced concrete slab, separated by independent vertical ventilated air cavities. The external cladding (the concrete slab) has sealed joints, which means that each air cavity is connected to the external environment only at the bottom and top of the façade. The height of the air cavity depends on the building elevation and on the presence of windows and/or protruding slabs. The TCC façade analyzed is part of the envelope on a residential 3-storey building located in the north of Italy, close to Brescia (Figure 2). In this case, the ventilated façade's height is equal to two storeys of the building (the ground floor has a different envelope system), which is the minimum height that allows us to gain some benefits from the natural ventilation inside the cavity of the façade, according to the literature. The thermal behaviour of the façade indicated in Figure 2 was monitored over one year, from August 2022 until August 2023 [29]. The results of this monitoring were used to calibrate and validate the CFD model described in this paper.

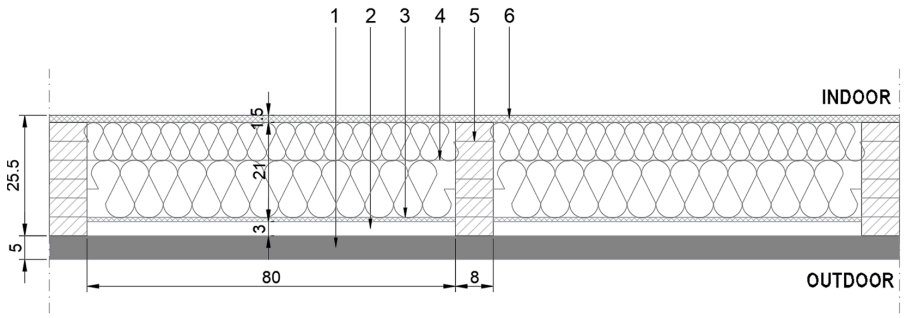

Figure 1. Horizontal section of the TCC façade studied (units in cm). The layers are (1) a reinforced concrete slab; (2) ventilated air cavity; (3) OSB panel; (4) rockwool insulation (100 kg/m^3); (5) timber-frame structure; and (6) an OSB panel. © Pastori S.

Figure 2. Monitored building, and illustration of the TCC ventilated envelope area analyzed (red dashed box). © Pastori S.

2.1. Geometry of the Model

A two-dimensional model was developed to study the façade behaviour (Figure 3). This choice was due to the need of keeping the model as simple as possible, and it was compatible with the geometry of the façade. In fact, since the air flows through many independent cavities, characterized by a limited width (80 cm), horizontal air flows are negligible. For this reason, a 2D façade model, which neglects the third spatial dimension, was adequate for the study purpose. Data supporting this assumption are included in Appendix C.

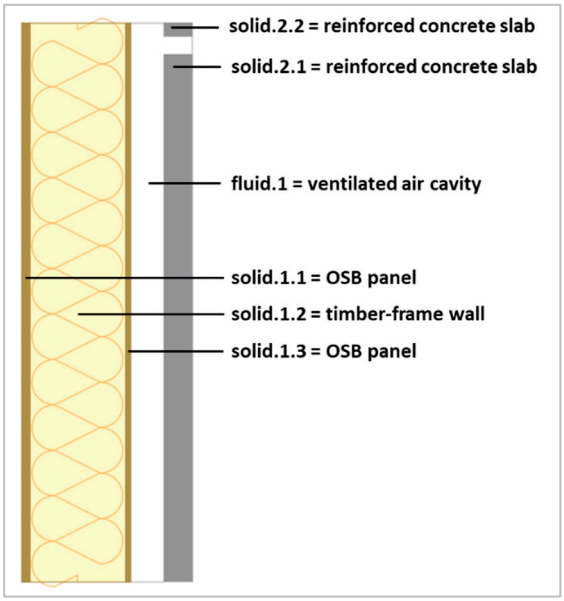

Figure 3. Naming of the regions used in the CFD model.

2.2. Physical Properties of the Model

The thermo-physical properties assigned to each material (i.e., each region) of the CFD model are reported in Table 1.

Table 1. Physical properties of each region of the CFD model.

Solid Regions						
Region		**Density (kg/m^3)**	**Thermal Conductivity (W/mK)**	**Specific Heat at Constant Pressure * (J/kgK)**	**Emissivity**	**Absorptivity**
Solid.1.1 = Internal OSB panel		550	0.100	1600	0.8	0.8
Solid.1.2 = Timber-frame insulated wall		100	0.035	1030	0.8	0.8
Solid.1.3 = External OSB panel		600	0.100	1600	0.8	0.8
Solid.2.1/.2.2 = Concrete slab		2400	2.00	1000	0.5	0.5
Fluid Region						
Region	**Density (kg/m^3)**	**Thermal Conductivity (W/mK)**	**Specific Heat at Constant Pressure (J/kgK)**	**Dynamic Viscosity (Pa s)**	**Molar Mass (kg/kmol)**	**Prandtl Number**
Air (properties at 30 °C)	Variable, function of temperature (incompressible ideal gas)	0.02588	1007	1.872×10^{-5}	28.966	0.728

* Values taken from EN ISO 10456 2007 [30].

2.3. Boundary Conditions

The boundary conditions applied to the model are described in this paragraph. Figure 4 shows the main boundary conditions applied to the CFD model. The temporal

evolution of the variables T_air,i (indoor air temperature), T_air,e (outdoor air temperature), qr_incident (solar irradiation incident on the facade), and V_air,e (air velocity at the bottom inlet of the cavity) were taken from the experimental monitoring. The values of hi (convective–radiative coefficient of indoor environment), he (convective–radiative coefficient of outdoor environment), and Rse (surface resistance of outdoor environment) were taken from the Standard ISO 6946 [31]. The values of T_outlet (air temperature at the top outlet of the cavity), P_outlet (air pressure at the top outlet of the cavity), and V_outlet (air velocity at the top outlet of the cavity) were calculated by the software during the simulation. A detailed model for wind flow was not included in the CFD analysis; in fact, as noticed during the experimental monitoring, the wind flow does not affect the façade thermal behaviour in a considerable way, given its high heat capacity. For this reason, only the air velocity at the bottom opening of the cavity was considered as the inlet condition for the fluid region. The complete setting of boundary conditions is reported in Appendix A.

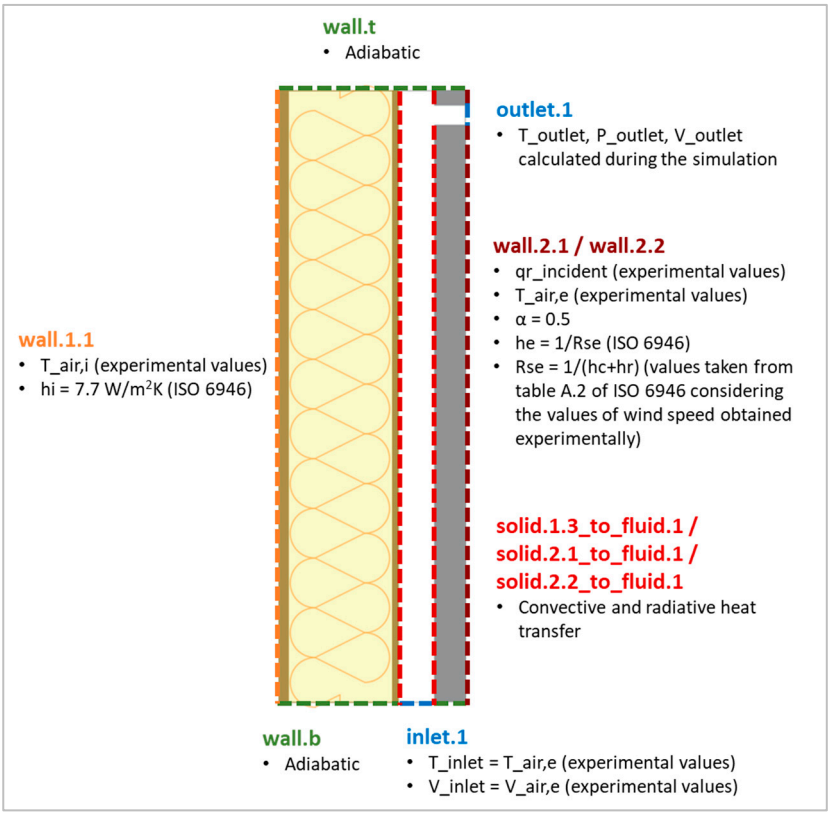

Figure 4. Main boundary conditions used in the CFD model.

2.4. Mesh Refinement Study

A mesh refinement study was performed to identify the best model discretization in terms of a trade-off between accuracy and computational cost. Three meshes were tested:

- m0012_baseMesh
- m0013_baseMeshx1.5
- m0014_baseMeshx1.5x1.5

The number of cells for each mesh was equal to the number in the previous one multiplied for 1.5 in both the vertical and horizontal directions. As expected, the results obtained showed that the grid refinement produces a slightly better accuracy, but with higher computational time. In this specific case, the improvement in the mesh accuracy did not produce consistent differences in the results, while the time needed for the computation increased considerably (see Table 2). For this reason, the mesh m0012 was chosen, and used for all future simulations. The geometry and mesh used are shown in Figure 5. The

first simulation (t0001) was run for 96 h in real-time (4 days), to see how long the model needed to catch the right temperature trends. The results of the first simulation showed that 48 h were enough for that, thus the second case (t0002) was run for only 48 h. The third simulation (t0003) was stopped after 24 h because of the huge amount of time needed.

Table 2. Results of the mesh refinement study.

Mesh Refinement Study					
Simulation	**Mesh**	**Solver**	**Time Simulated**	**Time Needed for Running Simulation**	**Temperatures That Differ More than 0.2 K from Base Case (t0001)**
t0001	m0012_baseMesh (7152 cells)	chtMultiRegionFoam	96 h (345,000 s)	67.5 h	-
t0002	m0013_baseMeshx1.5 (14,850 cells)	chtMultiRegionFoam	48 h (172,800 s)	100 h (+196% than t0001)	1.4%
t0003	m0014_baseMeshx1.5x1.5 (33,075 cells)	chtMultiRegionFoam	24 h (86,400 s)	314 h (+1761% than t0001)	5.7%

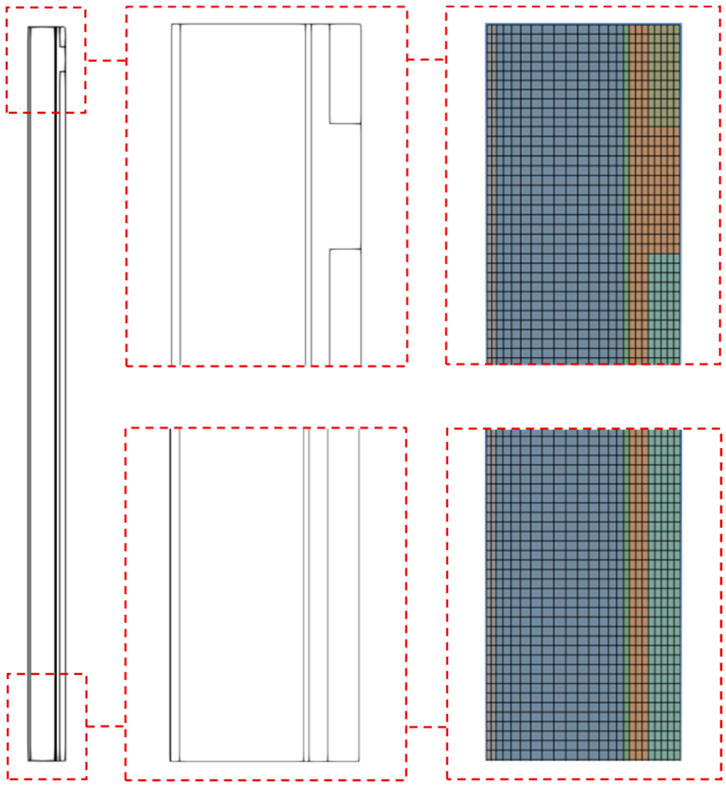

Figure 5. Geometry of and mesh within the 2D CFD model (colors indicate different regions).

2.5. Solver

The solver used, named "chtMultiRegionFoamIPPT" (a derivative of OpenFOAM® v2206's "chtMultiRegionFoam" solver, see Appendix A for details of the source code), allowed us to simulate transient fluid flow with heat transfer between regions. Buoyancy effects, turbulence, and radiation effects were also considered. The solver follows a segregated solution strategy, which means that the equations for each variable characterizing the system are solved sequentially, and the solution of the preceding equations is inserted in the subsequent equation. The coupling between fluid and solid regions follows the same strategy: First, the equations for the fluid are solved using the temperature of the solid of the preceding iteration to define the boundary conditions for the temperature in the fluid. After that, the energy equation for a solid region is solved using the temperature of the fluid of the preceding iteration to define the boundary condition for the solid temperature. This

iteration procedure is executed until convergence. For each fluid region the compressible Navier–Stokes equation is solved, while for the solid regions only the energy equation has to be solved. The regions are coupled with thermal boundary conditions considering radiation effects.

The original OpenFOAM® solver "chtMultiRegionFoam" was designed for transient simulations involving buoyant, turbulent fluid flows and solid heat conduction. It evolves all fields (i.e., velocity, pressure, temperature, turbulence if activated) for all regions at each time step. The adapted solver (i.e., "chtMultiRegionFoamIPPT") adds the sequential "freezing" and "unfreezing" of the flow solution to speed up the overall solution for the coupled equations. In detail, the adapted solver has the feature that the velocity and pressure fields for the fluid region(s) are not updated (i.e., "frozen") for a certain time period. This enables one to use much larger time steps when the flow is frozen, since a Courant number limitation no longer must be satisfied. Updating the pressure and velocity is expensive in terms of the computation time required, since a Poisson-like equation must be numerically solved in such an update. It is exactly this computational expense that is cut if the flow is "frozen". The solver is described in detail in the next section.

2.5.1. A New "Frozen–Unfrozen Flow" Solver

A novel algorithm, called the "frozen–unfrozen flow" solver, was developed to speed up the simulations, and consequently the overall model calibration process. The new solver switches the solution mode between "frozen" (i.e., no update of the velocity and pressure field, allowing large time steps) and "unfrozen" (i.e., solution of all transport equations, with normal time steps) cyclically. The normal time step in the "unfrozen" mode is determined by the Courant number and the solid diffusion numbers, while the time stepping in the "frozen" mode is set based on user input.

Figure 6 shows a schematic illustration of the cycling operation of the algorithm. It starts with the initial period (with duration $\tau_{initial}$), and then several cycles of unfrozen (red zones) and frozen (blue zones) modes are repeated till the end of the simulation. For stability reasons, a transition mode (the grey zones) must also be considered when the flow mode is switched between "frozen" and "unfrozen". The two periods of the cycle are characterized as follows:

- "Initial period": the fluid flow evolves with a time step calculated based on predefined Courant and solid diffusion numbers, to make the simulation stable at the beginning. It should be noted that the initial period not necessarily starts at time 0, since the algorithm is designed to work also in the case the simulation is re-started;
- "Normal period": the flow is sequentially set to the frozen and unfrozen modes.

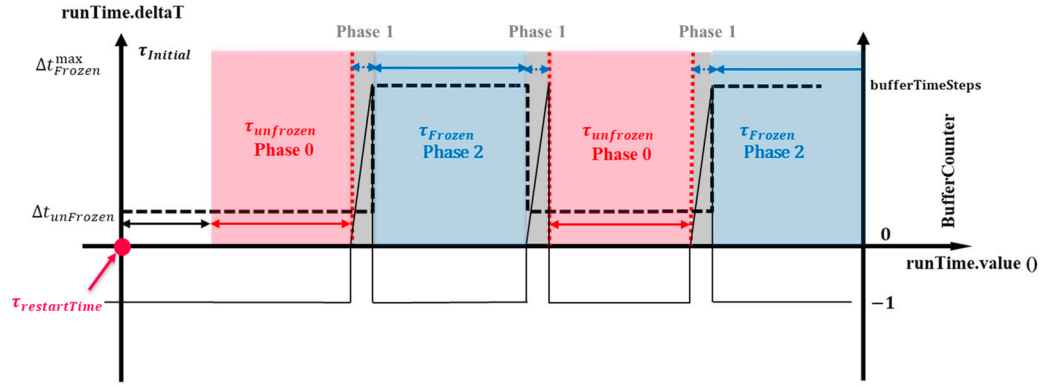

Figure 6. Illustration of the new solver algorithm.

Further algorithmic details related to these periods are summarized in Appendix B for interested readers.

2.5.2. Solver Performance Evaluation

To test the new solver's performance, new cases were created varying τ_{frozen} and $\tau_{unfrozen}$ (see Figure 6) in a systematic way to explore the effect of these numerical parameters on the accuracy of the results (i.e., the temperature values obtained in the model). Also, the amount of time needed for the computation was monitored. The new cases were compared to a base case, i.e., case t0001 which was identical to the new ones but run with the "old" solver. Table 3 summarizes the results obtained from the new cases, and documents the difference with the conventional CFD solver (i.e., the conventional solver) in the columns labelled with "% of values that differ more than…".

Table 3. List of cases run for testing the new solver and finding the optimal settings considering the trade-off between speed and accuracy of the results.

Comparison Between "Frozen-Unfrozen Flow" Solver and Conventional Solver							
Case	**tauFrozen/tauUnfrozen**	**Simulation Speedup (24 h in Real-Time Compared to Base Case t0001)**	**Relative Performance**	**Max Temperature Difference (K) from t0001**	**% of Values That Differ More than 0.2 K from t0001**	**% of Values That Differ More than 0.5 K from t0001**	**% of Values That Differ More than 1 K from t0001**
t0011	5 s/5 s = 1	x1.8	90%	−2.61 (at outlet.1)	12.9%	7.6%	3.9%
t0012	10 s/5 s = 2	x2.7	90%	3.61 (at outlet.1)	15.5%	8.0%	4.1%
t0013	15 s/5 s = 3	x3.5	88%	−2.87 (at outlet.1)	16.6%	7.7%	4.3%
t0014	50 s/5 s = 10	x9.4	85%	3.20 (at outlet.1)	12.4%	2.8%	1.0%
t0015	100 s/5 s = 20	x16.5	79%	2.66 (at outlet.1)	12.6%	2.9%	1.3%
t0016	500 s/5 s = 100	x45	45%	3.43 (at outlet.1)	20.8%	9.9%	4.5%

All the simulations were run for 24 h in real-time. $\tau_{initial}$ and Δt^{max}_{Frozen} were set equal to 1 s. The relative performance of the code, compared to the theoretical maximum performance that can be reached with the freeze/unfreeze setting used, was calculated as:

$$\text{Relative performance} = \text{simulation speedup}/(1 + \tau_{frozen}/\tau_{unfrozen}) \quad (1)$$

As expected, the simulation speed increased by increasing the ratio $\tau_{frozen}/\tau_{unfrozen}$, while the accuracy did not seem to be inversely proportional to the speed. The relative performance of the code shows how close the speed increase was to the theoretical optimum performance. For example, for case t0011, the new algorithm reaches almost the maximum performance of the code (i.e., 90% of the theoretical optimum). Instead, for case t0016, the relative performance was only at 45%, indicating a potential to further increase the observed speedup of x45.

We note in passing that a similar performance metrics were also measured for our 3D simulations presented in Appendix C (i.e., for $\tau_{frozen}/\tau_{unfrozen} = 20$ we obtain a 9.1x speedup in our 3D simulations).

2.6. Model Calibration

First, a sensitivity analysis was developed by comparing the results from the CFD model with the experimental data obtained. It consisted of changing the physical and numerical parameters used in the model such that the CFD results fit the experimental ones. The experimental data regarding the thermal behaviour of the façade during summer sunny days (from the 23 to 25 August 2022) were used as benchmark for the comparison. Details related to all relevant devices for experimental monitoring are available in Pastori's PhD thesis [29]. In all cases, the initial temperature fields close to the expected temperatures were considered to speed up the early temperature transients in the simulation.

The overview of the simulation runs of the sensitivity analysis is reported in Table 4. To run the cases the conventional solver was used, since the new solver was still under development at that point in time.

After the sensitivity analysis, the case that produced the lowest error in the results was considered as a starting point for the calibration process. The calibration consisted of changing one parameter of the model systematically and seeing how this change affected the final results. Calibration used the empirical data described in [29].

Table 4. Description of the cases run for the sensitivity analysis.

Sensitivity Analysis			
Case	**Goal**	**Physical Parameters**	**Boundary Conditions**
t0101	Base case	Parameters reported in Section 3.2	hToAmb = 1/Rse * hToAmbInt = 7.7 W/m^{2}K qrIncident: summer sunny days, south Ta: summer sunny days TaRad: off (=Ta) Ti: summer sunny days U: summer sunny days
t0102	Change in specific heat capacity for solid regions	2xCp of solid regions	hToAmb = 1/Rse * hToAmbInt = 7.7 W/m^{2}K qrIncident: summer sunny days, south Ta: summer sunny days TaRad: off (=Ta) Ti: summer sunny days U: summer sunny days
t0103	Change in solar irradiation values	20% reduction in incident solar irradiation values	hToAmb = 1/Rse * hToAmbInt = 7.7 W/m^{2}K qrIncident: 0.8xqr,summer sunny days, south Ta: summer sunny days TaRad: off (=Ta) Ti: summer sunny days U: summer sunny days
t0104	Change in emissivity values for solid regions	0.8x emissivity of solid regions	hToAmb = 1/Rse * hToAmbInt = 7.7 W/m^{2}K qrIncident: summer sunny days, south Ta: summer sunny days TaRad: off (=Ta) Ti: summer sunny days U: summer sunny days
t0105	Test how the model works with absence of solar irradiation	Incident solar irradiation switched off	hToAmb = 1/Rse * hToAmbInt = 7.7 W/m^{2}K qrIncident = 0 W/m^2 Ta: summer sunny days TaRad: off (=Ta) Ti: summer sunny days U: summer sunny days
t0106	Change the type of heat exchange between the external surface of the wall and the outdoor environment, considering convective and radiative heat exchange separately.	Outdoor convective and radiative heat transfers are considered separately: qcv = hcv (Ta − TC_ext) qrd = ε σ Fw-sky (TC_ext^4 − Tsky^4) Tsky = 0.037536 Ta$^{1.5}$ + 0.32 Ta	hToAmb = 1/Rse * hToAmbInt = 7.7 W/m^{2}K qrIncident: summer sunny days, south Ta: summer sunny days TaRad: Tsky. Csv Ti: summer sunny days U: summer sunny days
t0107	Change the type of heat exchange between the external surface of the wall and the outdoor environment, considering convective and radiative heat exchange separately.	Outdoor convective and radiative heat transfers are considered separately: qcv = hcv (Ta − TC_ext) qrd = ε σ Fw-sky (TC_ext^4 − Tsky^4) Tsky = 0.037536 Ta$^{1.5}$ + 0.32 Ta	hcvToAmb =4 + 4v * hToAmbInt = 7.7 W/m^{2}K qrIncident: summer sunny days, south Ta: summer sunny days TaRad: Tsky. Csv Ti: summer sunny days U: summer sunny days
t0108	Change the type of heat exchange between the external surface of the wall and the outdoor environment, considering convective and radiative heat exchange separately.	Option “hInclRad: false”	hToAmb = 1/Rse * hToAmbInt = 7.7 W/m^{2}K qrIncident: summer sunny days, south Ta: Ta,reduced.csv TaRad: off (=Ta) Ti: summer sunny days U: summer sunny days
t0109	Change specific heat capacity of solid regions	1.5xCp for solid regions	hToAmb = 1/Rse * hToAmbInt = 7.7 W/m^{2}K qrIncident: summer sunny days, south Ta: summer sunny days TaRad: off (=Ta) Ti: summer sunny days U: summer sunny days

Table 4. *Cont.*

Sensitivity Analysis			
Case	**Goal**	**Physical Parameters**	**Boundary Conditions**
t0110	Change in specific heat capacity of solid regions	2xCp for solid region 2 1xCp for solid region 1	hToAmb = 1/Rse * hToAmbInt = 7.7 W/m^{2}K qrIncident: summer sunny days, south Ta: summer sunny days TaRad: off (=Ta) Ti: summer sunny days U: summer sunny days
t0111	Change in thermal conductivity of solid regions	2xCp for solid region 2 1xCp for solid region 1 0.5xλ for solid regions	hToAmb = 1/Rse * hToAmbInt = 7.7 W/m^{2}K qrIncident: summer sunny days, south Ta: summer sunny days TaRad: off (=Ta) Ti: summer sunny days U: summer sunny days
t0112	Change in temperature values of outdoor air (Ta in °C) and specific heat capacity of solid regions	Ta,reduced = 0.6xTa 2xCp for solid region 2 1xCp for solid region 1	hToAmb = 1/Rse * hToAmbInt = 7.7 W/m^{2}K qrIncident: summer sunny days, south Ta: Ta,reduced TaRad: off (=Ta) Ti: summer sunny days, wall S3 U: summer sunny days, wall S3
t0113	Change in temperature values of outdoor air (Ta in °C)	TaReduced = 0.6xTa	hToAmb = 1/Rse * hToAmbInt = 7.7 W/m^{2}K qrIncident: summer sunny days, south Ta: Ta,reduced TaRad: off (=Ta) Ti: summer sunny days, wall S3 U: summer sunny days, wall S3
t0114	Change in temperature values of outdoor air (Ta in °C)	From 9 a.m. to 9 p.m.: TaReduced,version2 = 0.6xTa From 9 p.m. to 9 a.m.: TaReduced,version2 = 0.8xTa	hToAmb = 1/Rse * hToAmbInt = 7.7 W/m^{2}K qrIncident: summer sunny days, south Ta: Ta,reduced,version2 TaRad: off (=Ta) Ti: summer sunny days, wall S3 U: summer sunny days, wall S3
t0115	Change in temperature values of outdoor air (Ta in °C), specific heat capacity and thermal conductivity of solid region 2	TaReduced = 0.6xTa 1.5xCp for solid region 2 0.5xλ for solid region 2	hToAmb = 1/Rse * hToAmbInt = 7.7 W/m^{2}K qrIncident: summer sunny days, south Ta: Ta,reduced,version2 TaRad: off (=Ta) Ti: summer sunny days, wall S3 U: summer sunny days, wall S3
t0116	Change in temperature values of outdoor air (Ta in °C), specific heat capacity and thermal conductivity of solid region 2	From 9 a.m. to 9 p.m.: TaReduced,version2 = 0.6xTa From 9 p.m. to 9 a.m.: TaReduced, version2 = 0.8xTa 1.5xCp for solid region 2 0.5xλ for solid region 2	hToAmb = 1/Rse * hToAmbInt = 7.7 W/m^{2}K qrIncident: summer sunny days, south Ta: Ta,reduced,version2 TaRad: off (=Ta) Ti: summer sunny days, wall S3 U: summer sunny days, wall S3

* The Rse value was taken from EN ISO 6946 [31].

2.7. Model Validation

A validation process is necessary to test whether the calibrated CFD model also works for different boundary conditions. After the calibration of the CFD model against the experimental results collected for summer sunny days, the model was tested again considering cloudy summer days (48 h, i.e., from the 18th to the morning of the 20 August 2022; a detailed analysis of the deviation has been performed for the last 24 h).

3. Results

In what follows, the results obtained with the CFD model are presented and analyzed. The temperatures measured on the different surfaces of the facade are identified using the following abbreviations:

- TR: average temperature on the internal surface of the internal OSB panel;
- TO: average temperature on the surface towards the cavity of the external OSB panel;

- TC: average temperature on the concrete slab surface towards the ventilated cavity;
- TC_ext: average temperature on the external surface of the concrete slab.

The results of the sensitivity analysis and of the calibration process are also discussed. Ultimately, a comparison between the results obtained from the experimental monitoring and those given by the calibrated model is presented.

3.1. Sensitivity Analysis

Table 5 contains the results of the sensitivity analysis. The errors were calculated considering only the last 24h simulated, to exclude the transient part at the beginning of the simulations. The temperature TR is not reported in Table 5, since its values are predicted very well by the CFD model in all the cases run, with an error lower than 1% between the experimental values and the simulations. The reason for this almost perfect match is that TR is close to the indoor air temperature, which was applied as a boundary condition to the CFD model.

Table 5. List of the cases run in the sensitivity analysis, and error of the corresponding prediction for each case compared to the experimental results.

Results of the Sensitivity Analysis					
Case	**Time Needed for Running Simulation with Old Solver (h)**	**TO: Error % Between Experiment and CFD**	**TC: Error % Between Experiment and CFD**	**TC_ext: Error % Between Experiment and CFD**	**Average Error %**
t0101	37	12	10	9	10.33
t0102	32.5	8.75	4.96	10.97	8.23
t0103	36	13	10	7	10.00
t0104	36	12	10	8	10.00
t0105	41	19	18	13	16.67
t0106	39	18	18	16	17.33
t0107	39	18	18	18	18.00
t0108	33.5	14	14	13	13.67
t0109	32	10	7	9	8.67
t0110	31.5	8.85	5.19	11.00	8.35
t0111	30.5	9.41	5.49	12.57	9.16
t0112	28.5	10	6	9	8.33
t0113	30.5	12	8	5	8.33
t0114	30.75	11	8	6	8.33
t0115	27.25	12	7	9	9.33
t0116	29	11	6	9	8.67

3.2. Calibration Process

Starting from simulation t0104, the specific heat capacity (i.e., the cp value) of solid.2 (i.e., the concrete slab) was systematically changed. This was carried out to find the optimum value to minimize the error between the experimental value and the CFD prediction of temperature TO (i.e., the average temperature on the surface of the OSB panel towards the cavity). Simulation t0104 was chosen because it is one of the cases with a lower average error and a lower error in TO (see Table 6). Temperature TO was used as a reference because, together with TR, it determines the heat flux entering the building through the timber-frame wall. As already mentioned, the temperature TR is always well predicted by the CFD model in all the cases run during the sensitivity analysis. The results from the calibration simulations are shown in Table 6 and Figure 7.

According to the model, the lowest error in the temperature TO is 6.5% and corresponds to case t4500, which means that a cp = 4500 J/kgK should be considered for concrete. This value is 4.5 times higher than the reference value defined in Standard EN ISO 10456 [30]. This result is unrealistic and probably affected by a model deviation issue that leads to the prediction of low temperatures in the cavity (this issue is discussed in Section 3.4 below).

Table 6. Case description and results of the calibration simulations (cases considered for further analysis are highlighted in grey).

Results of Calibration Process				
Case	**Description**	**cp_concrete (J/kgK)**	**Error of TO Prediction**	**Note**
t1000 (=t0101)	1xCp_concrete_base	1000	11.59%	Cp value from EN ISO 10456:2007
t1500	1.5xCp_concrete_base	1500	9.97%	
t1750	1.75xCp_concrete_base	1750	9.38%	
t2000 (=t0104)	2xCp_concrete_bas	2000	8.85%	starting case
t2250	2.25xCp_concrete_base	2250	8.40%	
t2500	2.5xCp_concrete_base	2500	8.00%	
t3000	3xCp_concrete_base	3000	7.36%	
t3500	3.5xCp_concrete_base	3500	6.93%	
t4000	4xCp_concrete_base	4000	6.66%	
t4500	4.5xCp_concrete_b	4500	6.52%	best prediction
t5000	5xCp_concrete_base	5000	6.55%	
t6000	6xCp_concrete_base	6000	7.02%	

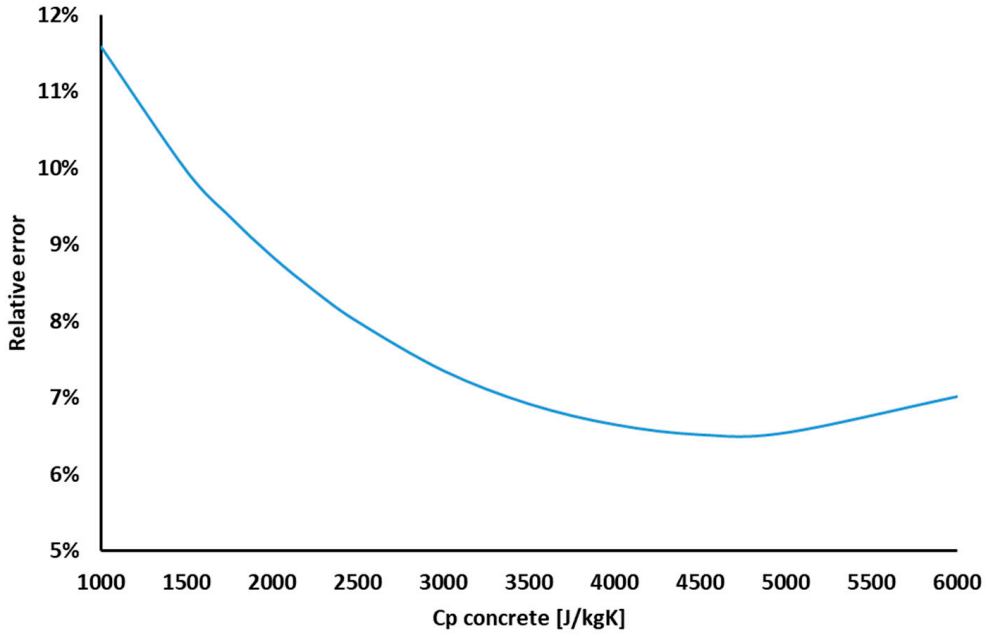

Figure 7. Graphical representation of the values listed in Table 6.

3.3. Validation Study

For the validation process, cases t2000 (i.e., the best case from the sensitivity analysis) and t4500 (i.e., the calibrated model case) were used. This was carried out to highlight whether the latter was more accurate than the former or not. The boundary conditions considered in this case refer to cloudy summer days, instead of the sunny summer days used for calibration. The models were run for 48 h; the average errors in the temperature prediction reported in Table 7 were calculated considering only the last 24 h, to exclude initialization effects. By looking at the results in Table 7, model t2000 predicts the experimental data with a lower error than the calibrated model t4500. However, the t4500 model's trend is more similar to the experimental one (Figure 8): if an offset of approximately 4 °C is considered for TO and TC, the experimental and simulated data would almost perfectly overlap. Similarly, an offset of approximately 1 °C for TC_ext would greatly reduce the error. This underprediction issue is discussed in the next section.

Table 7. Results of the validation study.

Results of Validation Process					
Case	**Error in TR Prediction**	**Error in TO Prediction**	**Error in TC Prediction**	**Error in TC_ext Prediction**	**Average Error**
t2000 (=t0104)	0.73%	13.99%	10.06%	8.14%	8.23%
t4500	0.73%	15.45%	11.91%	6.86%	8.74%

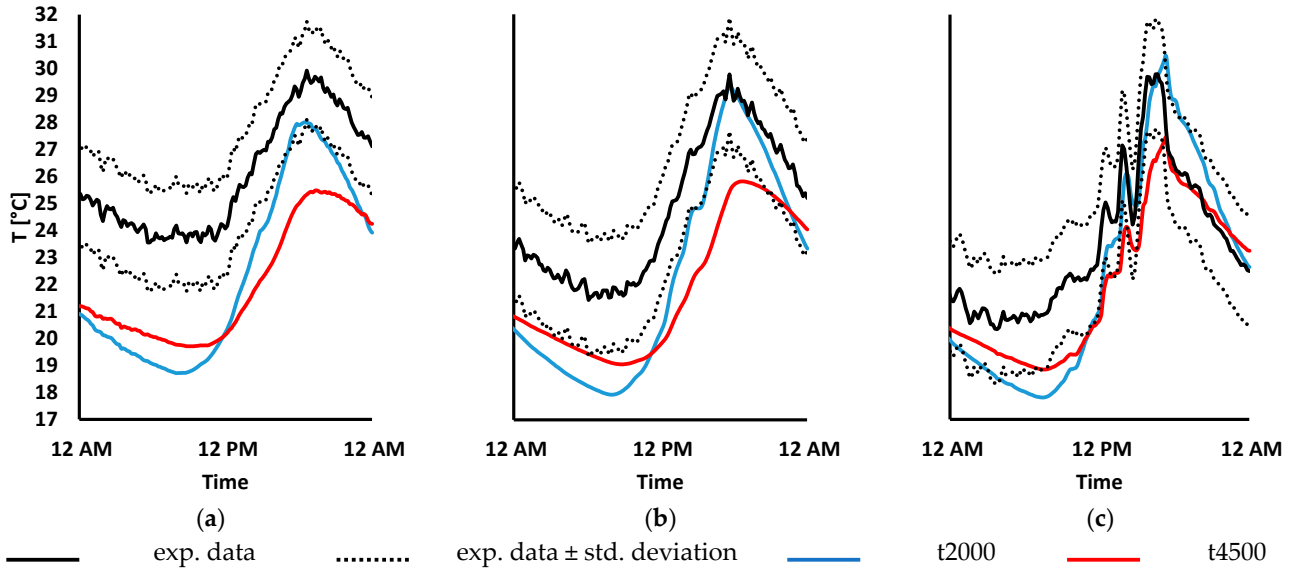

Figure 8. Prediction of (**a**) TO, (**b**) TC, and (**c**) TC_ext by model t2000 and t4500.

3.4. Discussion of the Temperature Underprediction Inside the Cavity

The persistent underprediction of the surface temperatures inside the cavity by the CFD simulation is probably caused by two effects: (i) an under-resolved flow, or (ii) a significantly incorrect assumption of the heat conductivity of the insulation material (i.e., the rockwool). While the latter is explored in Section 3.4.2 ("Effect of the heat conductivity of the rockwool insulation"), we next explore the possibility of an under-resolved flow, and what its relevance is when compared to radiative heat transfer.

3.4.1. Under-Resolved Flow and the Importance of Radiative Heat Transfer

A laminar flow was assumed in the cavity, but a relatively coarse computational mesh was used. Consequently, an instability might have developed in the flow and increased the thermal resistance, which was possibly not captured in the model. Thus, the heat transfer from the concrete to the OSB panel during heat up (i.e., at noon and in the early afternoon) is strongly underpredicted in the CFD model. During the cool-off phase (i.e., in the late afternoon) this leads to significantly lower temperature predictions in the air cavity, especially on the OSB panel surface.

The assumption of laminar flow in the cavity was motivated by the following reasons: the critical velocity of the flow transitions from laminar to turbulent (i.e., the range of the "transitional flow regime") was calculated based on a critical Reynolds number. Since there is not a single value for such a critical Reynolds number, but a range, critical velocities were calculated for the transitional flow regime: the critical velocity was 0.57 m/s for the lower limit (i.e., at the lower critical Reynolds number of Re_{low} = 2300) and 1.0 m/s for the upper limit (i.e., Re_{upper} = 4000). From the boundary conditions applied in our study (see Appendix A), a maximum fluid velocity in the cavity of 0.69 m/s and 0.79 m/s for the cloudy summer and sunny summer cases was observed, respectively. In addition, the

average velocity is 0.13 m/s and 0.24 m/s for the cloudy summer and sunny summer cases, respectively. Thus, the air velocity in the cavity is, during most of the time, well below the lower limit of the critical velocity, and always below the upper limit of the critical velocity. Moreover, it would be very challenging to use a correlation for turbulent flow in the transitional flow regimes since turbulent Nusselt number correlations were developed for fully turbulent flow conditions. Therefore, the flow in the air cavity was assumed to be laminar (see Appendix C for alternative results from a model that considered turbulence).

The transferred heat flux inside the cavity can be estimated via:

$$\dot{q} = \alpha_{HEx}\left(T_{wall} - T_{fluid}\right) \tag{2}$$

where

$$\begin{gathered} \alpha_{HEx} = Nu \cdot \left(\frac{\lambda_f}{D_h}\right) \\ D_h = 4A_c/P = \frac{4ab}{2(a+b)} \approx 2a \end{gathered} \tag{3}$$

$$\begin{gathered} Nu = 7.54 \; for \; T_{wall} = cte \\ Nu = 8.23 \; for \; \dot{q} = cte \end{gathered} \tag{4}$$

Equation (3) is taken from [32], and D_h indicates the hydraulic diameter. More correlations for the Nusselt number Nu are available in textbooks such as [12], specifically for turbulent and transitional flows. However, more advanced correlations do not change the message of the analysis, and should be treated with care as the flow in our case is not turbulent and only in rare situations transitional.

The cavity is modelled as a 2D domain with a width of 3 cm. Hence, the heat transfer coefficient for the cavity is calculated as follows if a fixed temperature at the walls is considered (i.e., $T_{wall} = cte$):

$$\alpha_{HEx} = Nu \cdot \frac{\lambda_f}{D_h} = 7.54 \cdot 0.02588/(2 \cdot 0.03) = 3.25 \; \mathrm{W/m^2K} \tag{5}$$

The average temperature of the cavity walls and air in the cavity needs to be calculated. These values have been obtained from cases t0104 and t4500 (see Figure 9). For an estimate of the patch-averaged heat fluxes due to heat transfer, two time snapshots were picked on this plot (i.e., at 8:00 a.m. and 6:00 p.m.). The averaged values have been obtained by the "integrate variables" feature in ParaView, which performs an area-weighted calculation. As can be seen in Table 8, the patch-average radiative and transferred heat flux are of similar magnitude. It should be noted that a negative radiative heat flux (i.e., q_r) means that radiative heat leaves the patch. The results in Table 8 indicate that both the emissivity of the wall and the details of the flow in the cavity are important when predicting the heat fluxes, and consequently the surface temperatures in the cavity. In summary, a (potentially) under-resolved flow can only partially explain the temperature underprediction in our CFD model since radiative transfer is also of considerable importance.

Table 8. Relative importance of radiative heat transfer inside the cavity for two different time snapshots for cases t0104 and t4500.

Time (s)	$T^{volume}_{fluid.1}$ (°C)	$T^{patch}_{solid.1.3}$ (°C)	$T^{patch}_{solid.2.1}$ (°C)	$\dot{q}$ Solid.1.3 to Fluid.1 (W/m^2)	$\dot{q}$ Solid.2.1 to Fluid.1 (W/m^2)	q_r Solid.1.3 (W/m^2)	q_r Solid.2.1 (W/m^2)
				case t0104			
6:00 p.m.	34.28	35.05	37.05	2.50	9.00	7.04	−9.73
8:00 a.m.	19.93	20.25	19.75	1.04	−0.59	−0.87	1.27
				case t4500			
6:00 p.m.	31.68	31.80	33.01	0.39	4.32	5.67	−6.09
8:00 a.m.	20.88	21.29	21.09	1.33	0.68	0.31	0.01

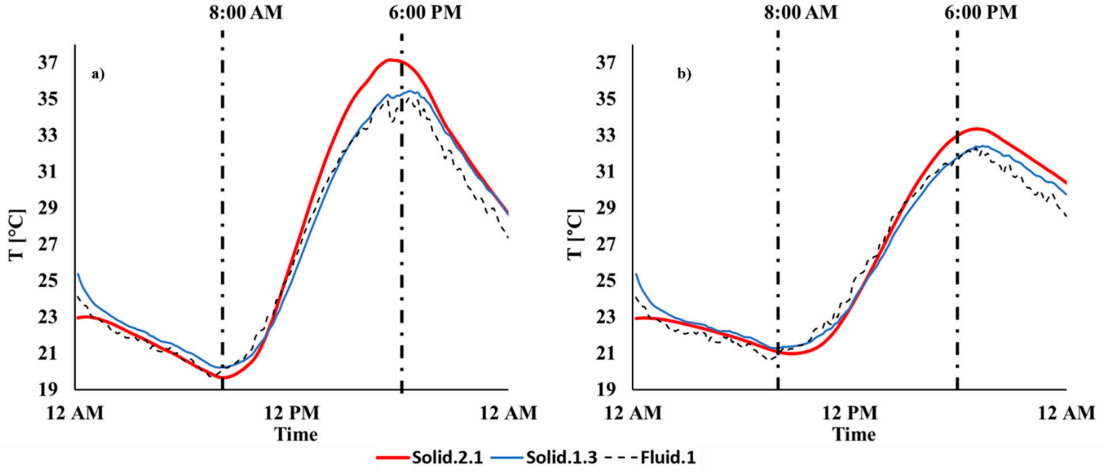

Figure 9. Volume-averaged temperature of fluid.1, as well as the patch-averaged temperature of solid2.1 and solid.1.3 for case t0104 (**a**), and case t4500 (**b**).

3.4.2. Effect of the Heat Conductivity of the Rockwool Insulation

Rockwool is part of the TCC system studied, and if this material becomes wet (e.g., due to condensation), it has a much higher heat conductivity compared to the nominal value in a dry state. Extreme increases in the rockwool's thermal conductivity by a factor of approximately 10 [33] to 50 [34] have been reported in the literature. We have explored the effect of such extreme increases in the thermal conductivity on our predictions, despite the fact that moisture was not observed during the experimental campaign. Specifically, we have chosen a 20-fold higher heat conductivity of the rockwool insulation (i.e., 0.7 [W/mK]) as in the base case.

The results for this scenario are depicted in Figure 10. Indeed, this simulation shows that the OSB panel's surface temperature ("TO") is much closer to the indoor temperature in a case where the rockwool is considered to be wet compared to the base case. Consequently, the agreement with the experimental data (see circles in Figure 10) is also improved. Similar conclusions can be drawn for the concrete surface temperature ("TC"). In summary, a higher heat conductivity of the rockwool could explain the difference between the experiment and the simulation to a large degree.

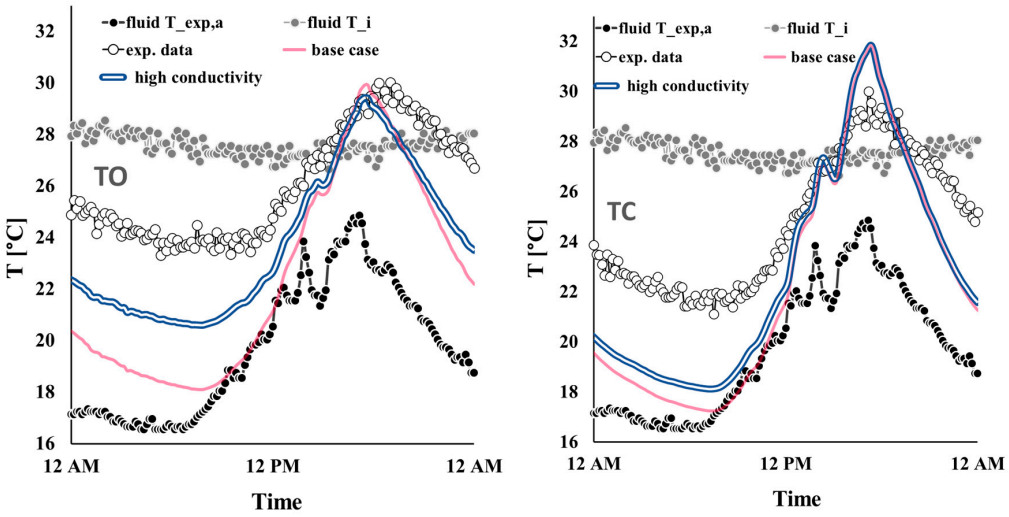

Figure 10. Comparison of experimental and simulation data at the surface of the OSB panel facing the cavity ("TO", left) and the concrete slab facing the cavity ("TC", right) for the base case (i.e., case t4500) and a case with high conductivity of the rockwool insulation. "T_exp,a" indicates the imposed outside air temperature, and "T_i" the indoor air temperature.

4. Conclusions

Starting from the data collected during an annual experimental campaign in the north of Italy, close to Brescia (described in [29]), the present paper focuses on the description and optimization of a multi-region CFD model. The experimental data collected were used for the calibration and validation of a 2D CFD model, which was developed and optimized for a specific envelope system. Several CFD models for the thermal analysis of ventilated facades were found in the literature, which were all tested and used to study ventilated facades with a thin external cladding. In contrast, the key innovative aspect of the current contribution was to develop and validate a simplified and optimized CFD model to analyze ventilated facades with external massive cladding. The model was developed in 2D to be as simple as possible, and it was optimized in terms of computational effort: a mesh refinement study was performed to select the optimal discretization. Also, a new "frozen–unfrozen flow" solver was implemented to allow faster simulations while still maintaining good accuracy of the results. The model was developed by using the open-source software OpenFOAM® v2206 to be accessible to everyone.

The validated model allowed us to obtain results with an accuracy around 92% (based on the average error of the temperature prediction compared to the experimental case; see values reported in Table 7). The deviation is mainly caused by the underprediction of the surface temperatures inside the façade's ventilated cavity. Solving this remaining issue would lead to an even higher model accuracy. As the aim of the study was the development of a fast CFD model, we have postponed more detailed studies in this direction until the future.

In the case that the newly implemented "frozen–unfrozen flow" solver is used, the simulations can be much faster than using the original solver: considering simulations for 24 h in real-time, the new solver allowed us to increase the speed of the simulation up to 45 times, keeping an acceptable error (i.e., <3.5 °C) in the results. This significant acceleration is impressive when considering the relatively simple modification of the algorithm. The analysis of the relative performance indicates that there is a trade-off between relative performance and speedup: while a simulation speedup of 45 times is achieved, there is still a potential of a ~55% increase in the relative performance. This potential might be realized in future studies to further increase the speed of the simulation, eventually leading to an even more impressive increase of x100. Also, the new algorithm was only benchmarked against a reference simulation using the same base CFD software, i.e., the native OpenFOAM® v2206 algorithm. Benchmarking versus other CFD software tools would be highly interesting in the future.

The calibrated CFD model can be used in the future to assess the thermal performance of TCC ventilated facades for different configurations, e.g., a different air cavity depth, concrete slab thickness, colour and material of the surfaces, orientation, or ventilation type (e.g., natural, forced, or closed cavity), etc. This would then allow for the analysis and optimization of building envelope solutions, partially avoiding the expensive and time-consuming construction of mock-ups. Specifically, mock-ups that are designed to study the effect of geometric parameters, different project locations (and hence boundary conditions), or different materials, could be replaced by the CFD model. In Appendix D we have documented exploratory simulations in this direction, specifically highlighting the effect of the thickness of a TCC façade. Accurate research in this respect might be interesting for systems manufacturers, in order to further develop their products to comply with the different projects' requirements, and for designers, to better choose and specify the systems to be used. Certainly, experiments for validation still remain key for benchmarking a CFD model's prediction. However, the new opportunities offered by calibrated CFD models for facades more than balance the efforts needed to create them from our perspective.

Also, the study is an important step towards digital twins for TCC ventilated facades, since the calibrated CFD model can make predictions faster than real-time [35]. For example, the model might be used together with advanced control strategies to minimize a building's

energy consumption. Also, the simulated data might be useful in a refined energy flow analysis, e.g., to identify the major mechanisms of heat transfer to the outdoor environment.

Unfortunately, any calibrated CFD model requires experimental data for calibration and validation. Any measurement inaccuracy, or poorly assumed boundary condition leads to limitations. Also, a 1:1 digital twin of the façade is required, which might necessitate the digitalization of existing buildings. Future work might address these limitations, e.g., through a refined validation study or a sensitivity analysis with respect to assumed boundary conditions to mitigate these limitations. Another direction for future improvement could be to use a one-dimensional model (for both the fluid and solid regions) to further speed up the simulations.

At a broader level, the research aimed to contribute to our knowledge regarding the thermal performance of ventilated facades composed of an internal lightweight wall structure and an external massive cladding.

Author Contributions: Conceptualization, S.P. and S.R.; methodology, S.P., S.R. and M.-S.S.; software, M.-S.S.; validation, S.P.; formal analysis, S.P. and M.-S.S.; investigation, S.P.; resources, S.R.; data curation, S.P. and M.-S.S.; writing—original draft preparation, S.P. and M.-S.S.; writing—review and editing, S.R. and E.S.M.; visualization, S.P. and M.-S.S.; supervision, S.R. and E.S.M.; project administration, S.P. and S.R.; funding acquisition, S.R. All authors have read and agreed to the published version of the manuscript.

Funding: Supported by TU Graz Open Access Publishing Fund.

Data Availability Statement: The original data presented in the study are openly available via https://gitlab.tugraz.at/13097018C9D61E3C/chtMultiRegionTools (accessed on 1 August 2024).

Acknowledgments: Open Access Funding by the Graz University of Technology.

Conflicts of Interest: The authors declare no conflicts of interest. The funders had no role in the design of the study; in the collection, analyses, or interpretation of data; in the writing of the manuscript; or in the decision to publish the results.

Disclaimer: OPENFOAM® is a registered trademark of OpenCFD Limited, producer and distributor of the OpenFOAM software via https://www.openfoam.com/, accessed on 1 August 2024. This offering is not approved or endorsed by OpenCFD Limited, producer and distributor of the OpenFOAM software via https://www.openfoam.com/, accessed on 1 August 2024, and owner of the OPENFOAM® and OpenCFD® trade marks.

Appendix A. Settings of the CFD Solver and Boundary Conditions

The basic settings of the CFD solver were as follows:

OpenFOAM® v2206 (from https://www.openfoam.com/, accessed on 1 August 2024)

Solver: chtMultiRegionFoamIPPT (adapted version with "frozen-unfrozen" solver routine)

Courant- and Diffusion-number-based adaptive time stepping (Co_{max} = 1, Di_{max} = 20, Δt_{max} = 5 [s])

Laminar flow (no turbulence model was used; see Appendix C for the effect of a turbulence model)

Upwind schemes for all fluid field quantities

Linear (second order accurate) schemes for all diffusive quantities

PIMPE (transient) simulation of fluid flow using one outer corrector, and two inner (pressure) correction loops

Details of the radiation solver are as follows:

View-factor-based calculation with fully transparent air in the cavity region

Ten flow iterations per radiation iteration

No face agglomeration

The complete setting used for the boundary conditions is described in Table A1. Plots showing the temporal evolution of the boundary conditions considered are presented in Figures A1 and A2.

Table A1. Complete setting of the boundary conditions applied to the model.

Region	Variable	Boundary Conditions Applied
wall.1.1	Temperature	externalWallHeatFluxTemperatureIPPT (user defined) Ti: indoor air temperature, .csv file with values from experimental monitoring TiRad: off (i.e., indoor mean radiant temperature is switched off and only Ti is considered for the heat exchange between the wall and the indoor ambient) hInclRad: true (i.e., the radiation to indoor ambient lumped into the heat transfer coefficient hCoeffs taken from UNI EN ISO 6946) hCoeffs: heat transfer coefficient, .csv file with hCoeffs = 7.7 [W/m^{2}K] (value for indoor ambient taken from UNI EN ISO 6946)
wall.2.* (wall.2.1 wall.2.2)	Temperature	externalWallHeatFluxTemperatureIPPT Ta: outdoor air temperature, .csv file with monitored values TaRad: off (i.e., outdoor mean radiant temperature is switched off and only Ta is considered for the heat exchange between the wall and the outdoor environemnt) hInclRad: true (i.e., the radiation to outdoor ambient lumped into the heat transfer coefficient hCoeffs taken from UNI EN ISO 6946) hCoeffs: heat transfer coefficient, .csv file with h = 1/Rse (Rse values taken from UNI EN ISO 6946, table A.2 according to the wind speed registered during the experimental monitoring) qr: incident solar irradiation on the wall, .csv file with values from experimental monitoring qrRelaxation: 1
solid.1.*_to_solid.1.* (solid.1.1_to_solid.1.2 solid.1.2_to_solid.1.3)	Temperature	compressible::turbulentTemperatureRadCoupledMixed kappaMethod: solidThermo (for values of thermophysical properties see Table 1 of main document) no radiative radiation model because of direct contact
solid.*_to_fluid.1 fluid.1_to_solid.* (solid.1.3_to_fluid.1 solid.2.1_to_fluid.1 solid.2.2_to_fluid.1 fluid.1_to_solid.1.3 fluid.1_to_solid.2.1 fluid.1_to_solid.2.2)	Temperature	compressible::turbulentTemperatureRadCoupledMixed kappaMethod: solidThermo or fluidThermo (for values of thermophysical properties see Table 1 of main document)
	Pressure	fixedFluxPressure p0: 10^5 [Pa]
	Radiation	greyDiffusiveRadiationViewFactor qro: uniform 0 for emissivity values see Table 1 of main document
	Velocity	noSlip
inlet.1	Temperature	uniformFixedValue uniformValue: .csv file with Ta values
	Pressure	zeroGradient
	Radiation	greyDiffusiveRadiationViewFactor qro: uniform 0 emissivity: 0.9
	Velocity	uniformFixedValue uniformValue: .csv file with values from experimental monitoring
outlet.1	Temperature	inletOutlet inletValue: 297 [K]
	Pressure	fixedValue value: 10^5 [Pa]
	Radiation	greyDiffusiveRadiationViewFactor qro: uniform 0 emissivity: 0.9
	Velocity	inletOutlet inletValue: (0 0 0) [m/s]
wall.t wall.b	Temperature	zeroGradient

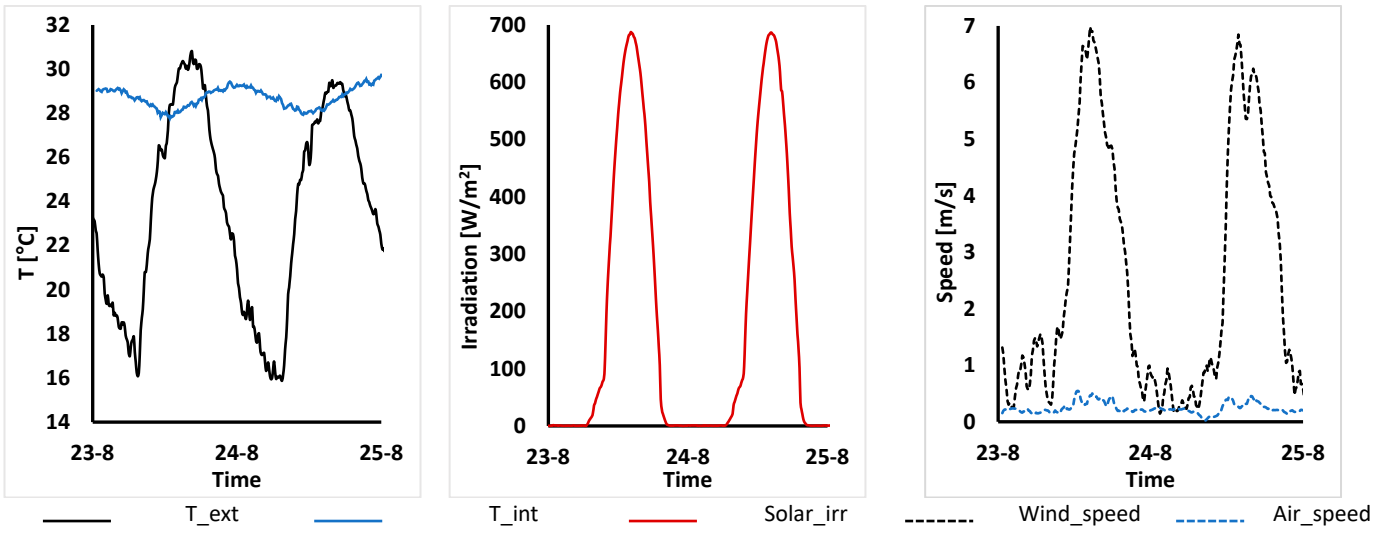

Figure A1. Temporal evolution of the boundary conditions considered for summer sunny days: outdoor temperature (T_ext), indoor temperature (T_int), incident solar irradiation on the façade (Solar_irr), wind speed (Wind_speed), and air speed at the bottom opening of the ventilated cavity (Air_speed).

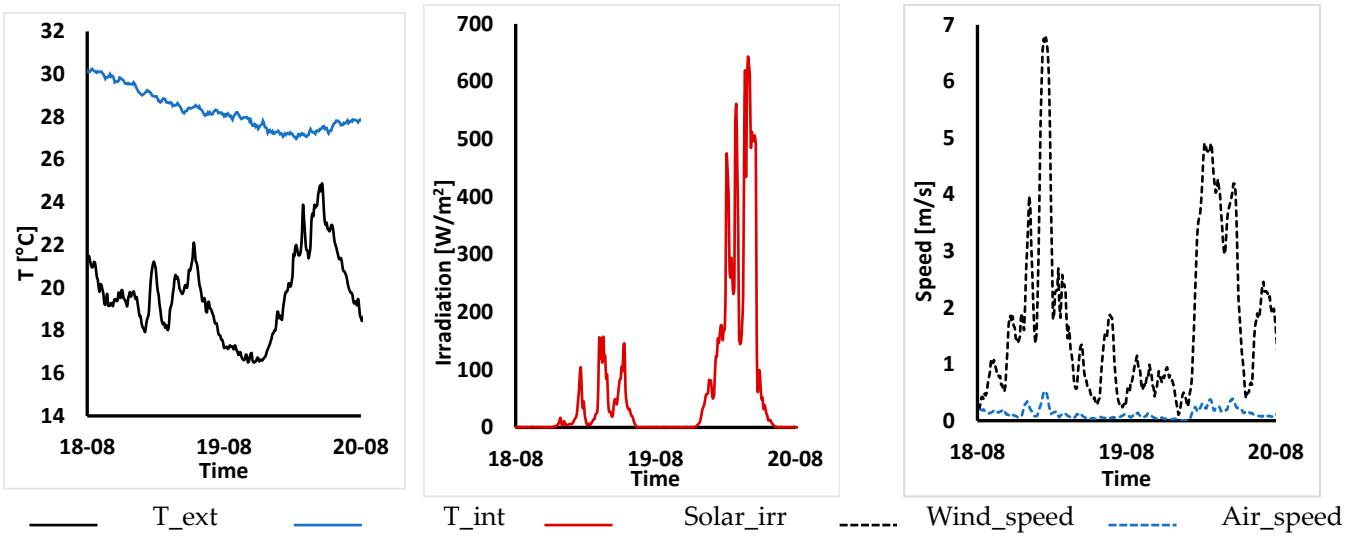

Figure A2. Temporal evolution of the boundary conditions considered for summer cloudy days (the meaning of the colours is identical to that in Figure A1).

Appendix B. Algorithmic Details of the "Frozen–Unfrozen Flow" Solver

In this appendix, more information about the algorithm for the "frozen–unfrozen flow" solver are given.

The Initial period is the timespan when the simulation starts from 0 (or from the latest saved time steps in case of simulation restart) and ends at the end of the specified initial time duration (i.e., $\tau_{initial}$) defined in the "fluid.1/fvSolution" file. The algorithm in this period has the following features (see also Figure A3):

- Declaration of the variables;
- Calculation of the time-step based on courant and solid diffusion numbers;
- Setting the unfrozen mode for the fluid flow;
- Setting the "cycleStartTime" at the end of this period.

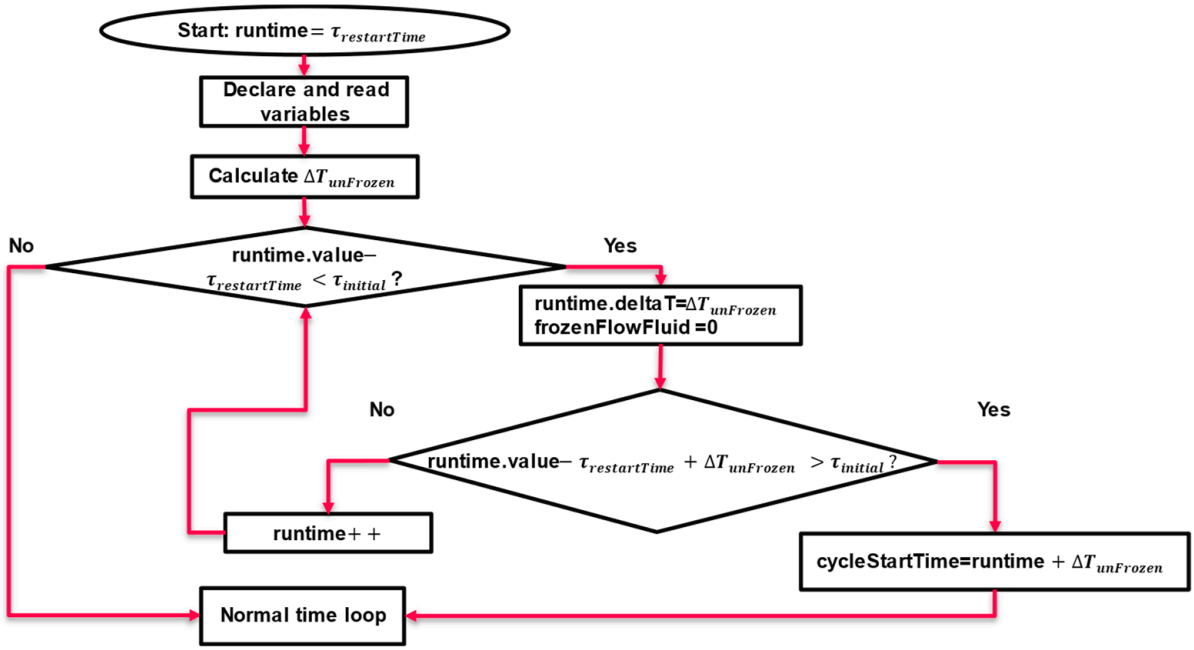

Figure A3. The algorithm for the initial period ($\tau_{initial}$) in the new solver.

The normal period when the flow solution mode is sequentially set to unfrozen and frozen. The sum of the frozen time (τ_{Frozen}) and unfrozen time ($\tau_{unFrozen}$) is called a cycle. The maximum time step ($\Delta t^{frozen}{}_{max}$), τ_{Frozen} and $\tau_{unFrozen}$ are user settings and are given in "fluid.1/fvSolution".

This period has the following features (see Figures A4 and A5):

- It calculates the current time in a cycle ("currentTimeInCycle"), which is the difference between the current flow time and "cycleStartTime".
- It assigns the phases for frozen, unfrozen, or transition modes (see Figures A4 and A5):
  - If "bufferCounter" is equal to −1 and the runtime is in unfrozen mode, the phase is 0, otherwise, the phase is 2.
  - If "bufferCounter" is not equal to −1, then set the phase to 1.
- If the phase is "0", then set the time step to $\Delta t_{unFrozen}$ and the mode of the flow "unfrozen". If the new flow time falls in a new phase, set "bufferCounter" to 0 and store the latest flow solution mode as "frozenFlowFluidOld".
- If the phase is 1, then set the time step to $\Delta t_{unFrozen}$, then decide based on the previous phase flow mode:
  - If "frozenFlowFluidOld" is unfrozen and "bufferCounter" reaches the use input value (i.e., "bufferCounterSteps"), set the time step to Δt^{Max}_{Frozen} and "bufferCounter" to −2.
  - If "frozenFlowFluidOld" is frozen and "bufferCounter" reaches the use input value (i.e., "bufferCounterSteps"), then "bufferCounter". to −2 and set "cycleStartTime" =current flow time + $\Delta t_{unFrozen}$.
- If the phase is 2 then, freeze the flow and set the time step to Δt^{Max}_{Frozen}. Once the solution falls out of the cycle, set "bufferCounter" to 0 and store the latest flow solution mode as "frozenFlowFluidOld".
- Repeat the above steps till the flow time reaches the end time of the simulation (defined in "controlDict").

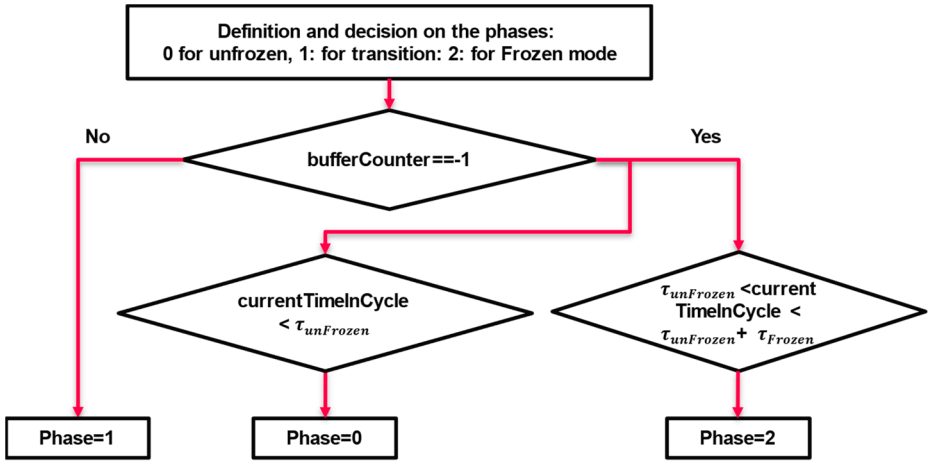

Figure A4. An illustration of the steps in the solver algorithm defining the phases.

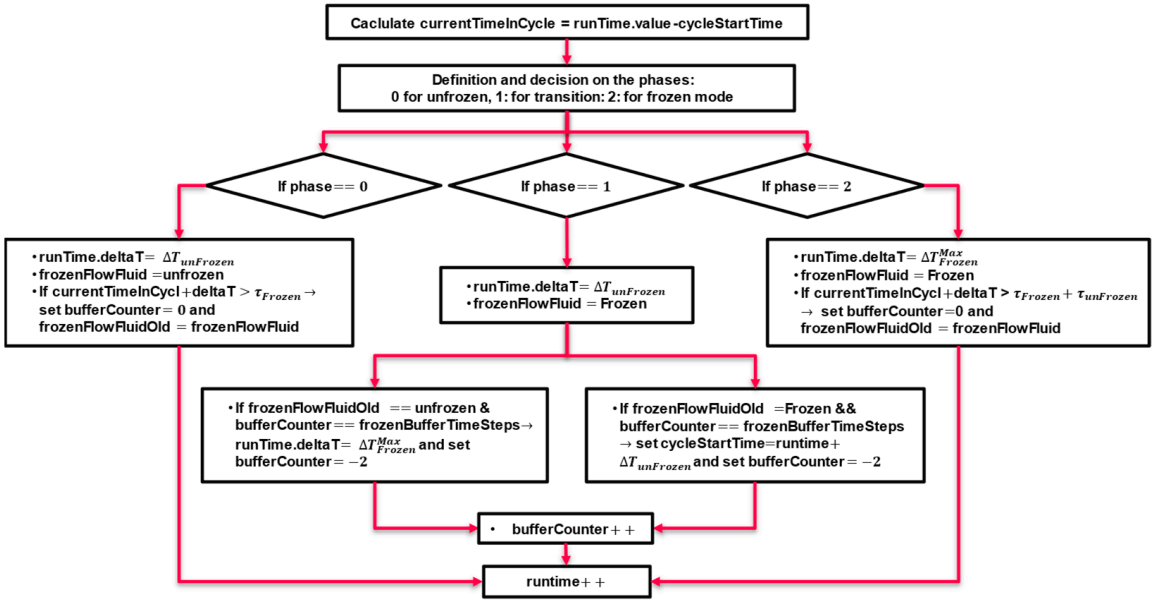

Figure A5. Illustration of the "normal period" for the solver algorithm.

Appendix C. Effect of a Turbulence Model and a 3D Domain

Figure A6 illustrates the effect of using a turbulence model (i.e., the "realizable k-ε" model available in OpenFOAM®). This simulation was based on the scenario defined by case t4500 (see Section 3.3 "Validation study"). As can be seen, absolutely no visual difference can be observed between the cases with and without the turbulence model, which is supported by the very small turbulent viscosity ν_t (see rightmost panel in Figure A6). As can be seen by the latter, turbulence is observed only near the outlet of the fluid region and with a low intensity (the molecular viscosity is approximately $1.6{\cdot}10^{-5}$ [m^2/s], which is higher than the turbulent viscosity in most regions of the cavity).

To support our argument on using a 2D simulation domain, we here compare the results of a 2D and an explorative 3D simulation. The latter considered a 0.5 [m] deep slab of the façade discretized by 40 mesh elements giving a similar spatial resolution as in the x-direction. Three-dimensional simulations are extremely expensive, and hence could not be run for the total 48 h of the experimental dataset in a reasonable time. Consequently, only the qualitative differences between these two types of simulation domain are summarized in Figure A7. Effects due to a 3D domain are small in general. However, as can be seen, there are two differences between 2D and 3D simulation results:

(a) Near the top right outlet of the cavity, the 2D model features a locally higher temperature in the OSB panel facing the cavity. This is not present in the 3D model due to slight differences in the handling of view factors in the radiation model (i.e., in the 3D model view factors were considered in larger regions for performance reasons). This results in a more homogeneous temperature distribution in the y-direction in the 3D simulation compared to the data from the 2D model.

(b) The fluid temperature field in the 3D simulation shows a small variation in the depth in the (z-)direction in the region near the fluid outlet (see rightmost panel of Figure A7). This is caused by a somewhat chaotic flow in this region (data available via our gitlab repository, see the "Data Availability Statement"). However, this 3D flow feature has no consequences on the heat transfer inside the cavity.

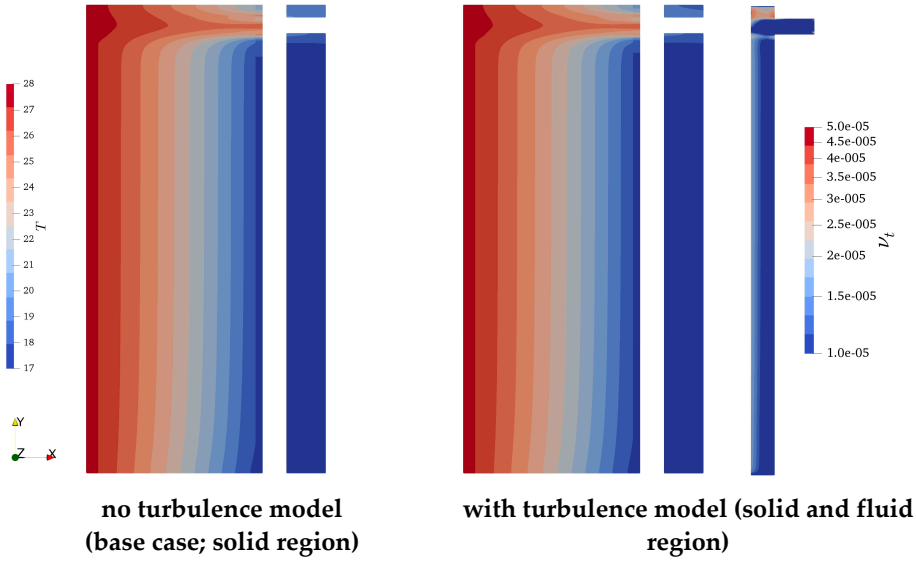

Figure A6. Effect of a turbulence model in comparison to the base case results (i.e., case t4500) on the solid temperature distribution (data at 8:00 a.m. is shown; the figure has been scaled in the y-direction for better representation; in the rightmost panel the predicted turbulent viscosity is illustrated).

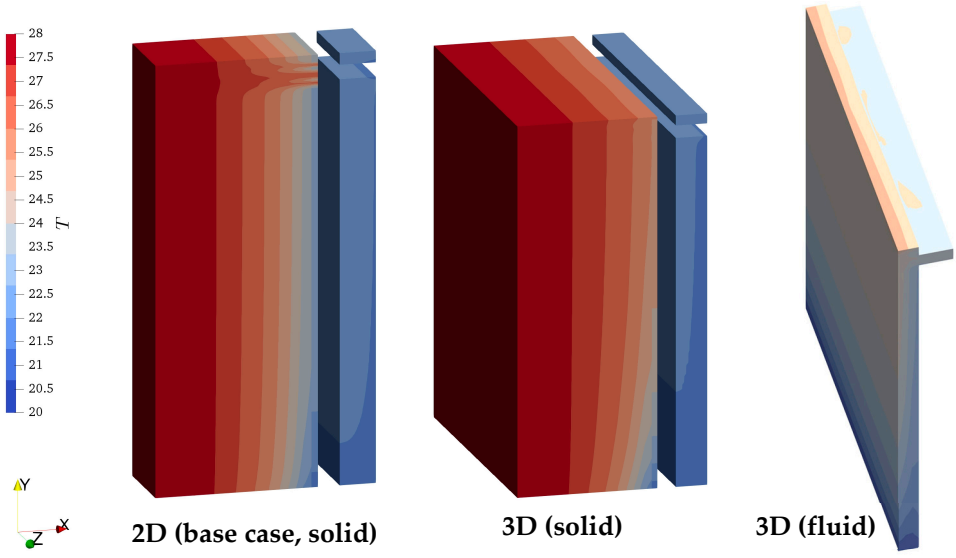

Figure A7. Effect of using a 3D computational domain in comparison to the base case results (i.e., case t4500) on the solid and fluid temperature distribution (data at time t = 120 [min] is shown; the figure has been scaled in the y-direction for better representation).

In summary, the 3D effects can be considered minimal, and only of marginal consequence for the thermal behaviour of the façade.

Appendix D. Effect of the Thickness of the TCC Layers

To study effect of the thickness of the TCC layers, we performed simulations in which we simply scaled the whole setup (i.e., solid and fluid regions) in the *x*-direction. These simulations were based on the scenario defined by case t4500 (see Section 3.3 "Validation study"). Specifically, we have performed simulations considering a "double thickness", and a "half thickness" geometry.

Results for the time evolution of key temperatures (i.e., that at the surface of the OSB panel "TO", and the concrete surface facing the cavity "TC") are illustrated in Figure A8. Clearly, the TCC's thickness has a significant effect on (i) the peak temperatures at the surface (i.e., more extreme temperatures in case of the "half thickness" geometry) and (ii) the temporal evolution of the temperature (i.e., significant damping of high frequency temperature fluctuations caused by variations in the solar irradiation in case of "double thickness" case).

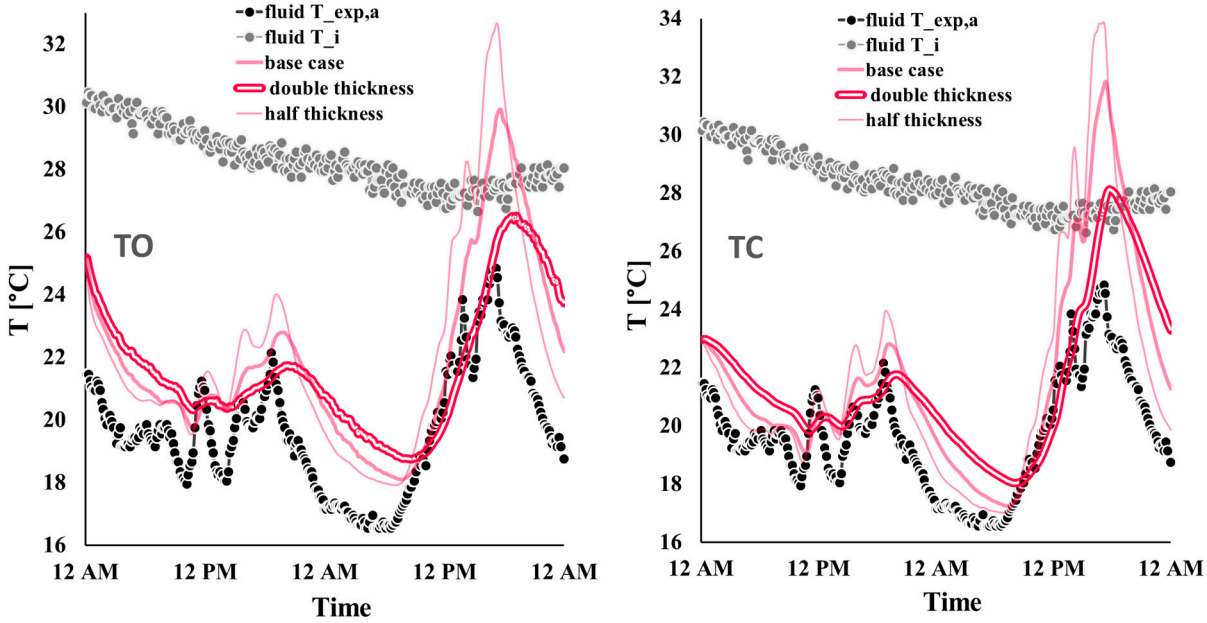

Figure A8. Effect of different TCC layer thicknesses on the temperatures facing the cavity ("base case" refers to case t4500).

References

1. Asdrubali, F.; Ferracuti, B.; Lombardi, L.; Guattari, C.; Evangelisti, L.; Grazieschi, G. A Review of Structural, Thermo-Physical, Acoustical, and Environmental Properties of Wooden Materials for Building Applications. *Build. Environ.* **2017**, *114*, 307–332. [CrossRef]
2. Janssen, H. Characterization of Hygrothermal Properties of Wood-Based Products—Impact of Moisture Content and Temperature. *Constr. Build. Mater.* **2018**, *185*, 39–43. [CrossRef]
3. Fortuna, S.; Mora, T.D.; Peron, F.; Romagnoni, P. Environmental Performances of a Timber-Concrete Prefabricated Composite Wall System. *Energy Procedia* **2017**, *113*, 90–97. [CrossRef]
4. Pastori, S.; Mereu, R.; Mazzucchelli, E.S.; Passoni, S.; Dotelli, G. Energy Performance Evaluation of a Ventilated Façade System through Cfd Modeling and Comparison with International Standards. *Energies* **2021**, *14*, 193. [CrossRef]
5. Destro, R.; Boscato, G.; Mazzali, U.; Russo, S.; Peron, F.; Romagnoni, P. Structural and Thermal Behaviour of a Timber-Concrete Prefabricated Composite Wall System. *Energy Procedia* **2015**, *78*, 2730–2735. [CrossRef]
6. Patania, F.; Gagliano, A.; Nocera, F.; Ferlito, A.; Galesi, A. Thermofluid-Dynamic Analysis of Ventilated Facades. *Energy Build.* **2010**, *42*, 1148–1155. [CrossRef]
7. Giancola, E.; Sanjuan, C.; Blanco, E.; Heras, M.R. Experimental Assessment and Modelling of the Performance of an Open Joint Ventilated Façade during Actual Operating Conditions in Mediterranean Climate. *Energy Build.* **2012**, *54*, 363–375. [CrossRef]

8. Ciampi, M.; Leccese, F.; Tuoni, G. Ventilated Facades Energy Performance in Summer Cooling of Buildings. *Sol. Energy* **2003**, *75*, 491–502. [CrossRef]
9. Giancola, E.; Sánchez, M.N.; Friedrich, M.; Larsen, O.K.; Nocente, A.; Avesani, S.; Babich, F.; Goia, F. Possibilities and Challenges of Different Experimental Techniques for Airflow Characterisation in the Air Cavities of Façades. *J. Facade Des. Eng.* **2018**, *6*, 34–48. [CrossRef]
10. Gagliano, A.; Nocera, F.; Aneli, S. Thermodynamic Analysis of Ventilated Façades under Different Wind Conditions in Summer Period. *Energy Build.* **2016**, *122*, 131–139. [CrossRef]
11. Stazi, F.; Ulpiani, G.; Pergolini, M.; Magni, D.; Di Perna, C. Experimental Comparison Between Three Types of Opaque Ventilated Facades. *Open Constr. Build. Technol. J.* **2018**, *12*, 296–308. [CrossRef]
12. Incropera, F.P.; Dewitt, D.P.; Bergman, T.L.; Lavine, A.S. *Fundamentals of Heat and Mass Transfer*, 6th ed.; John Wiley & Sons: Hoboken, NJ, USA, 2007; ISBN 978-0-471-45728-2.
13. Jensen, J.; Bartak, M.; Drkal, F. Modeling and Simulation of a Double-Skin Facade System. *ASHRAE Trans.* **2007**, *108*, 1251–1259.
14. Manz, H. Numerical Simulation of Heat Transfer by Natural Convection in Cavities of Facade Elements. *Energy Build.* **2003**, *35*, 305–311. [CrossRef]
15. Xamán, J.; Álvarez, G.; Lira, L.; Estrada, C. Numerical Study of Heat Transfer by Laminar and Turbulent Natural Convection in Tall Cavities of Façade Elements. *Energy Build.* **2005**, *37*, 787–794. [CrossRef]
16. Pappas, A.; Zhai, Z. Numerical Investigation on Thermal Performance and Correlations of Double Skin Façade with Buoyancy-Driven Airflow. *Energy Build.* **2008**, *40*, 466–475. [CrossRef]
17. Pasut, W.; De Carli, M. Evaluation of Various CFD Modelling Strategies in Predicting Airflow and Temperature in a Naturally Ventilated Double Skin Faade. *Appl. Therm. Eng.* **2012**, *37*, 267–274. [CrossRef]
18. Safer, N.; Woloszyn, M.; Roux, J.J. Three-Dimensional Simulation with a CFD Tool of the Airflow Phenomena in Single Floor Double-Skin Facade Equipped with a Venetian Blind. *Sol. Energy* **2005**, *79*, 193–203. [CrossRef]
19. Sanjuan, C.; Suárez, M.J.; González, M.; Pistono, J.; Blanco, E. Energy Performance of an Open-Joint Ventilated Façade Compared with a Conventional Sealed Cavity Façade. *Sol. Energy* **2011**, *85*, 1851–1863. [CrossRef]
20. Baldinelli, G. Double Skin Façades for Warm Climate Regions: Analysis of a Solution with an Integrated Movable Shading System. *Build. Environ.* **2009**, *44*, 1107–1118. [CrossRef]
21. Srebric, J.; Chen, Q.; Glicksman, L.R. A Coupled Airflow-and-Energy Simulation Program for Indoor Thermal Environment Studies (RP-927). *ASHRAE Trans.* **2000**, *106*, 465–476.
22. Zhai, Z.J.; Chen, Q.Y. Performance of Coupled Building Energy and CFD Simulations. *Energy Build.* **2005**, *37*, 333–344. [CrossRef]
23. Brandl, D.; Mach, T.; Grobbauer, M.; Hochenauer, C. Analysis of Ventilation Effects and the Thermal Behaviour of Multifunctional Façade Elements with 3D CFD Models. *Energy Build.* **2014**, *85*, 305–320. [CrossRef]
24. Horikiri, K.; Yao, Y.; Yao, J. Modelling Conjugate Flow and Heat Transfer in a Ventilated Room for Indoor Thermal Comfort Assessment. *Build. Environ.* **2014**, *77*, 135–147. [CrossRef]
25. Fantucci, S.; Marinosci, C.; Serra, V.; Carbonaro, C. Thermal Performance Assessment of an Opaque Ventilated Façade in the Summer Period: Calibration of a Simulation Model through in-Field Measurements. *Energy Procedia* **2017**, *111*, 619–628. [CrossRef]
26. Hajdukiewicz, M. Formal Calibration Methodology Relating to Cfd Models of Naturally Ventilated Internal Environments. Ph.D. Thesis, NUI Galway, Galway, Ireland, 2013.
27. Laitinen, A.; Saari, K.; Kukko, K.; Peltonen, P.; Laurila, E.; Partanen, J.; Vuorinen, V. A Computational Fluid Dynamics Study by Conjugate Heat Transfer in OpenFOAM: A Liquid Cooling Concept for High Power Electronics. *Int. J. Heat Fluid Flow* **2020**, *85*, 108654. [CrossRef]
28. Chourdakis, G.; Schneider, D.; Uekermann, B. OpenFOAM preCICE: Coupling OpenFOAM with External Solvers for Multi-Physics Simulations. *OpenFOAM J.* **2023**, *3*, 1–25. [CrossRef]
29. Pastori, S. Timber-Concrete Composite Ventilated Envelope Systems. Experimental and Numerical Investigations for Thermal Performance Control and Optimization. Ph.D. Thesis, Politecnico di Milano, Milan, Italy, 2024.
30. *EN ISO 10456:2007*; Materials and Products—Hygrothermal Properties—Tabulated Design Values and Procedures for Determining Declared and Design Thermal Values. ISO Central Secretariat: Geneva, Switzerland, 2007.
31. *EN ISO 6946:2017*; Components and Building Elements—Thermal Resistance and Thermal Transmittance—Calculation Methods. ISO Central Secretariat: Geneva, Switzerland, 2017.
32. Kays, W.M.; Crawford, M.E. *Convective Heat and Mass Transfer*; Cambridge University Press: Cambridge, UK, 1980.
33. Antepara, I.; Fiala, L.; Pavlik, Z.; Cerny, R. Moisture Dependent Thermal Properties of Hydrophilic Mineral Wool: Application of the Effective Media Theory. *Mat. Sci.* **2015**, *21*, 449–454. [CrossRef]
34. Lu, F.; Kaviany, M.; Williams, J.; Addison-Smith, T. Heat, mass and momentum transport in wet mineral-wool insulation: Experiment and simulation. *Int. J. Heat Mass Trans.* **2024**, *228*, 125644. [CrossRef]
35. Tahmasebinia, F.; Lin, L.; Wu, S.; Kang, Y.; Sepasgozar, S. Exploring the Benefits and Limitations of Digital Twin Technology in Building Energy. *Appl. Sci.* **2023**, *13*, 8814. [CrossRef]